Wave interaction with subwavelength resonators

Habib Ammari

Department of Mathematics, ETH Zürich

Subwavelength resonances

- Focus, trap, and guide waves at subwavelength scales.

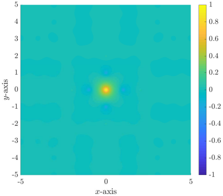

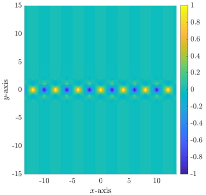

- Microstructured resonant media: Building block microstructure: subwavelength resonator.
- Subwavelength resonators: size $<$ resonant wavelength
  - Monopolar subwavelength resonators: Helmholtz resonators and Minnaert bubbles;
  - Dipolar subwavelength resonators: decorated membrane resonators and plasmonic particles;

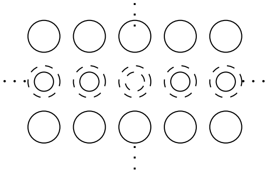

Monopolar subwavelength resonators

- Model:

$$\begin{cases} \Delta u + \omega^2 \dfrac{\rho}{\kappa} u = 0 \quad \text{in} \quad \mathbb{R}^d \setminus \overline{D}, d = 2, 3, \\ \Delta u + \omega^2 \dfrac{\rho_b}{\kappa_b} u = 0 \quad \text{in} \quad D, \\ u|_+ = u|_- \quad \text{on} \quad \partial D, \\ \dfrac{1}{\rho} \dfrac{\partial u}{\partial \nu}\Big|_+ = \dfrac{1}{\rho_b} \dfrac{\partial u}{\partial \nu}\Big|_- \quad \text{on} \quad \partial D, \\ u^s := u - u^{in} \text{ satisfies the (outgoing) Sommerfeld radiation condition.} \end{cases}$$

- ρ_b, ρ, κ_b, κ: material parameters inside and outside D; positive.
- $v = \sqrt{\kappa/\rho}$; $v_b = \sqrt{\kappa_b/\rho_b}$; $k = \omega\sqrt{\rho/\kappa}$; $k_b = \omega\sqrt{\rho_b/\kappa_b}$.
- $k_b/k = O(1)$; High contrast: $\delta := \rho_b/\rho \ll 1$.
- Subwavelength resonance: Associated wavelength several orders of magnitude larger than the size of D.
- Strong monopole scattering of waves.

Dipolar subwavelength resonators

- Model:

$$
\begin{cases}
\Delta u + \omega^2 \frac{\rho}{\kappa} u = 0 \quad \text{in} \quad \mathbb{R}^d \setminus \overline{D}, \\
\Delta u + \omega^2 \frac{\rho_b(\omega)}{\kappa_b} u = 0 \quad \text{in} \quad D, \\
u|_+ = u|_- \quad \text{on} \quad \partial D, \\
\frac{1}{\rho} \frac{\partial u}{\partial \nu}\Big|_+ = \frac{1}{\rho_b(\omega)} \frac{\partial u}{\partial \nu}\Big|_- \quad \text{on} \quad \partial D, \\
u^s := u - u^{in} \text{ satisfies the (outgoing) Sommerfeld radiation condition.}
\end{cases}
$$

- κ_b, κ: positive; $\kappa_b/\kappa = O(1)$;
- ρ_b: frequency dependent with negative real part over certain frequency ranges;
- Subwavelength resonance: Associated wavelength several orders of magnitude larger than D.
- Strong dipole scattering of waves.

Super-resolution

- Resolution: smallest detail that can be resolved.
- $G_{k,V}$: outgoing fundamental solution of the Helmholtz operator:

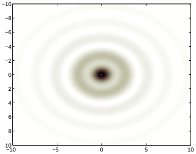

$$\Delta + k^2 + V(x).$$

- V: compactly supported.
- $\min_x \int_{|y|=R} |G_{k,V}(x,y) - G_{k,V}(y,x_0)|^2 ds(y).$
- Helmholtz-Kirchhoff identity[1]:

$$\Im m\, G_{k,V}(x,x_0) = k \int_{|y|=R} \overline{G_{k,V}(y,x_0)} G_{k,V}(x,y) ds(y) \quad \text{as } R \to +\infty.$$

- $\Rightarrow$ Resolution: determined by the behavior of the imaginary part of the Green function of the medium.

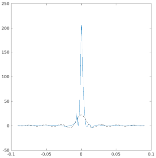

- $\Im m\, G_{k,V}$: point spread function.
- The more point-like $\Im m\, G_{k,V}$ is, the sharper the resolution.

[1] with J. Garnier, W. Jing, H. Kang, M. Lim, K. Sølna, H. Wang, Springer 2013.

Band gap opening

- Floquet transform:
  - $\mathcal{U}[f](x,\alpha) = \sum_{n\in\mathbb{Z}^d} f(x-n)e^{i\alpha\cdot n}$.
  - $\alpha \in$ Brillouin zone $\mathbb{R}^d/(2\pi\mathbb{Z}^d)$.

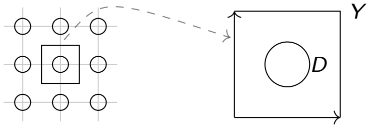

- Spectral theorem for a self-adjoint, elliptic operator L with periodic coefficients:

$$\sigma(L) = \bigcup_{\alpha\in\mathbb{R}^d/(2\pi\mathbb{Z}^d)} \left[\min_{\alpha} \mu_l(\alpha), \max_{\alpha} \mu_l(\alpha)\right], L(\alpha)[f] = \mathcal{U}[L[f]];$$

$(\mu_l(\alpha))_l$:discrete spectra of $L(\alpha)$.

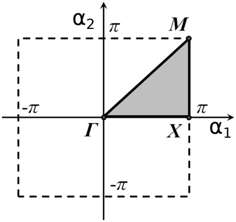

Brillouin zone

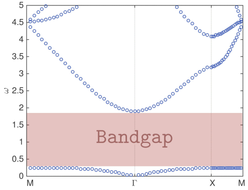

Bloch dispersion curves

Microstructured resonant media

- Dilute regime (Small-volume fraction of the subwavelength resonators): Effective medium theory:
  - High contrast materials: slightly below the free space resonant frequency of a single resonator $\Rightarrow$ Super-resolution.
  - Negative effective refractive index $\Rightarrow$ Subwavelength band gap opening slightly above the free space resonant frequency.
  - Double negative metamaterials[2]: dimers of subwavelength resonators.

[2] Metamaterials: composites made of tailored building blocks that are composed of one or more constituent bulk materials with material properties going beyond those of the ingredient materials, qualitatively or quantitatively.

Microstructured resonant media

- Non-dilute regime: High-frequency homogenization techniques
  - Super-resolution slightly below a critical frequency.
  - Subwavelength band gap opening slightly above a critical resonance.
  - Critical frequency $\neq$ free space resonant frequency.
  - Defect modes:
    - Point defect: trapped in a defected resonator;
    - Line defect: Localized to and guided along the line of defected resonators.
- Topological properties: Stability with respect to imperfections.

Monopolar subwavelength resonances

- Monopolar resonance frequency for a subwavelength resonator of arbitrary shape[3]:

$$\underbrace{\sqrt{\frac{\mathrm{Cap}_D}{|D|}} v_b \sqrt{\delta}}_{:=\omega_M(\delta)} + i \underbrace{\left(-\frac{\mathrm{Cap}_D^2 v_b^2}{8\pi v |D|}\delta\right)}_{:=\gamma} + O(\delta^{\frac{3}{2}}).$$

- Capacity $\mathrm{Cap}_D := \int_{\partial D} \mathcal{S}_D^{-1}[1]\, d\sigma$; $\mathcal{S}_D$: Single-layer potential associated with the fundamental solution G to the Laplacian: $\mathcal{S}_D[\phi] = \int_{\partial D} G(x-y)\phi(y)\, d\sigma(y)$.
- Monopole approximation near the monopolar resonance frequency:

$$u^s(x) = g(\omega, \delta, D)(1 + O(\omega) + O(\delta) + o(1))u^{in}(x_0) G_k(x, x_0).$$

- G_k: outgoing fundamental solution of the Helmholtz operator $\Delta + k^2$.
- Scattering coefficient g:

$$g(\omega, \delta, D) = \frac{\mathrm{Cap}_D}{1 - (\frac{\omega_M}{\omega})^2 + i\gamma}.$$

- Scattering enhancement near the monopolar resonance frequency.

[3] with B. Fitzpatrick, D. Gontier, H. Lee, H. Zhang, Ann. IHP C, 2018.

Monopolar subwavelength resonances

- Integral formulation: $\mathcal{A}(\omega, \delta)[\Psi] = F$;
- 0: characteristic value of the limiting operator-valued function: $\omega \mapsto \mathcal{A}(\omega, 0)$.

- Gohberg-Sigal theory:
  - V: complex neighborhood of 0:

$$\omega_M(\delta) = \frac{1}{2\pi i}\mathrm{tr} \int_{\partial V} \omega \mathcal{A}(\omega, \delta)^{-1} \frac{\partial}{\partial \omega} \mathcal{A}(\omega, \delta)\, d\omega.$$

  - Muller's method: compute characteristic eigenvalues.

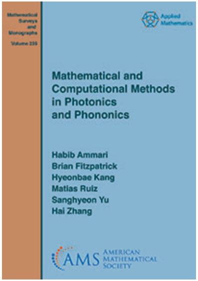

Super-resolution

- Dilute regime: When excited slightly below the monopolar resonance frequency ω_M a large number of small subwavelength resonators acts as a medium with high-contrast effective κ in which super-resolution is achievable[4]:

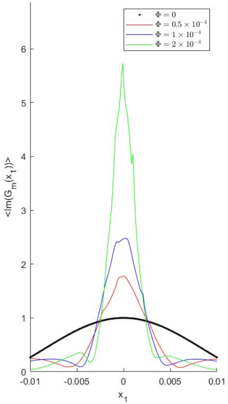

[4]with B. Fitzpatrick, D. Gontier, H. Lee, H. Zhang, Proc. Royal Soc. A, 2017.

Subwavelength band gap opening

- Dilute regime: When excited slightly above the monopolar resonance frequency ω_M a large number of small subwavelength resonators acts as a medium with a negative effective κ $\Leftarrow$ subwavelength band gap opening.

- Band structure of a square array of circular resonators with radius $R = 0.05$ and contrast $\delta^{-1} = 5000$:

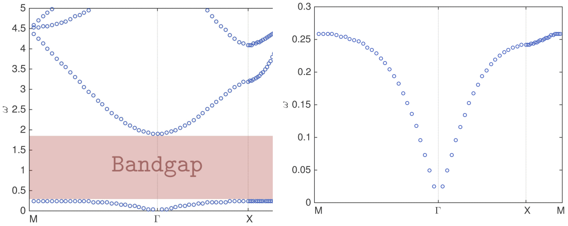

Effective medium theory

- Effective operator[5]:

$$\Delta + k^2 + V(x); \qquad V(x) = \frac{1}{(\frac{\omega_M}{\omega})^2 - 1} \Lambda \widetilde{V}(x).$$

  - Λ: depends only on the size and number of the subwavelength resonators;
  - $\widetilde{V}$: depends only on the distribution of the centers of the subwavelength resonators.
- ω slightly below ω_M: high-contrast effective κ;
- ω slightly above ω_M: negative effective κ;
- Effective medium theory: does not hold at $\omega = \omega_M$.

[5] with H. Zhang, SIAM J. Math. Anal., 2017.

Super-resolution in high-contrast media

- Mechanism of Super-resolution in high-contrast media[6,7]:
  - Modal decomposition of the effective Green function $G_{k,V}$:
    - Mixing of modes: intrinsic nature of non-hermitian systems.
  - Interaction of the point source x_0 with the resonant structure excites modes in the decomposition of $G_{k,V}$ that are oscillating at subwavelength scales: subwavelength resonance modes:
    - Subwavelength resonance modes excited $\Rightarrow$ dominate over the other ones in the modal expansion of $G_{k,V}$.
    - $\Im m\, G_{k,V}$ may have sharper peak than the free-space one due to the excited subwavelength resonant modes.
  - Super-resolution:
    - only limited by the resonant structure and the signal-to-noise ratio in the data.
    - only occurs for a discrete set of frequencies.

[6] with J. Garnier, J. de Rosny, K. Sølna, Inverse Problems, 2014.
[7] with H. Zhang, Proc. Royal Soc. A, 2015; Comm. Math. Phys., 2015.

Subwavelength band gap opening

- Non-dilute regime:
  - Subwavelength band gaps[8]: appear slightly above $\omega_* \neq \omega_M$.
  - Super-resolution[9]: appear slightly below ω_*.
  - High-frequency homogenization.
- Band structure of a square array of circular resonators with radius $R = 0.25$ and contrast $\delta^{-1} = 1000$:

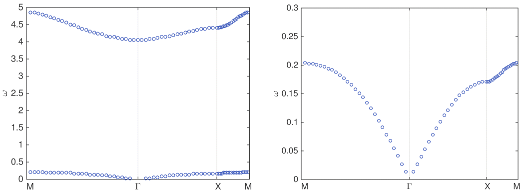

[8]with B. Fitzpatrick, H. Lee, S. Yu, H. Zhang, J. Diff. Equat., 2017.
[9]with H. Lee, H. Zhang, SIAM J. Math. Anal., 2018.

Subwavelength band gap opening

- Asymptotic behavior of ω_1^α:
  - For $\alpha \neq 0$ and sufficiently small δ,

$$\omega_1^\alpha = \omega_M \sqrt{c_\alpha} + O(\delta^{3/2});$$

  - ω_M: free space subwavelength resonant frequency;
  - $c_\alpha := \mathrm{Cap}_{D,\alpha} / \mathrm{Cap}_D$;
  - Quasi-periodic capacity:

$$\mathrm{Cap}_{D,\alpha} := -\int_{\partial D} \underbrace{(\mathcal{S}_D^{\alpha,0})^{-1}[1]}_{\psi_\alpha} \, d\sigma.$$

  - $\mathcal{S}_D^{\alpha,k}$: Single layer potential associated with quasi-periodic Green's function:

$$G^{\alpha,k}(x,y) = \sum_{n \in \mathbb{Z}^3} \frac{e^{i(2\pi n + \alpha)\cdot(x-y)}}{k^2 - |2\pi n + \alpha|^2}.$$

  - $\mathcal{S}_D^{\alpha,k}[\phi] = \int_{\partial D} G^{\alpha,k}(x,y)\phi(y)\, d\sigma(y).$

Subwavelength band gap opening

- D: symmetric with respect to planes $\{(x_1, x_2, x_3) : x_j = 0\}$, $j = 1, 2, 3 \Rightarrow \mathrm{Cap}_{D,\alpha}$ and ω_1^α attain their maxima at $\alpha^* = (\pi, \pi, \pi)$ (ω_1^α attained at the corner M of the Brillouin zone).
- For $\epsilon > 0$ small enough,

$$\mathrm{Cap}_{D,\alpha^*+\epsilon\tilde{\alpha}} = \mathrm{Cap}_{D,\alpha^*} + \epsilon^2 \Lambda_D^{\tilde{\alpha}} + O(\epsilon^4).$$

- $\Lambda_D^{\tilde{\alpha}}$: negative semi-definite quadratic function of $\tilde{\alpha} \Rightarrow$

$$\frac{v_b^2}{|D|} \Lambda_D^{\tilde{\alpha}} = - \sum_{1 \leq i,j \leq 3} \lambda_{ij} \tilde{\alpha}_i \tilde{\alpha}_j.$$

- (λ_{ij}): symmetric and positive semi-definite.

Subwavelength band gap opening

- s: period of the crystal; $\delta = O(s^2)$.
- $\omega_*^s = (1/s)\omega_*^1$; Critical frequencies $= O(1)$ as $s \to 0$.
- Near the critical frequency ω_*^s: eigenfunctions can be decomposed into two parts[10]:
  - One part: slowly varying and satisfies a homogenized equation;
  - Second part: periodic across each elementary crystal cell and is varying.
- $(\omega_*^s)^2 - \omega^2 = O(s^2)$; Asymptotic of Bloch eigenfunction $u_{1,s}^{\alpha^*/s+\tilde{\alpha}}$:

$$u_{1,s}^{\alpha^*/s+\tilde{\alpha}}(x) = \underbrace{e^{i\tilde{\alpha}\cdot x}}_{\text{macroscopic behavior}} \underbrace{S\left(\frac{x}{s}\right)}_{\text{microscpic behavior}} + O(s);$$

- Macroscopic plane wave $e^{i\tilde{\alpha}\cdot x}$ satisfies:

$$\sum_{1\leq i,j\leq 3} \lambda_{ij}\partial_i\partial_j \tilde{u}(x) + \frac{\omega_*^2 - \omega^2}{\delta}\tilde{u}(x) = 0.$$

[10] with H. Lee, H. Zhang, SIAM J. Math. Anal., 2018.

Subwavelength band gap opening

- $(\omega_*^s)^2 - \omega^2 = \beta\delta$;
- $\sum_{1\leq i,j\leq 3} \lambda_{ij}\tilde{\alpha}_i\tilde{\alpha}_j = \beta + O(s^2)$:
  - $\beta > 0 \Rightarrow$ plane wave Bloch eigenfunction:
    - Homogenized equation for the bubbly phononic crystal;
    - Microscopic field: periodic and varies on the scale of s;
    - Microscopic oscillations of the field at the period of the crystal justify the super-resolution phenomenon.
  - $\beta < 0 \Rightarrow$ exponentially growing or decaying functions $\Rightarrow$ band gap opening.

Subwavelength band gap opening

- One-dimensional plot along the $x-$axis of the real part of the Bloch eigenfunction of the square lattice shown over many unit cells:

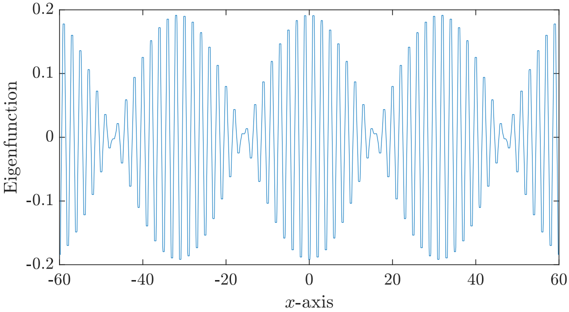

Subwavelength defect modes

- Defect modes: Create a detuned resonator with an upward shifted resonance frequency (within the subwavelength band gap).
  - Dilute regime: weak interaction $\Rightarrow$ decrease the radius of one resonator (from R to $R + \epsilon$; $\epsilon < 0$);
  - Non-dilute regime: strong interaction $\Rightarrow$ increase the radius of one resonator (from R to $R + \epsilon$; $\epsilon > 0$);
  - Shift at resonator radius $=$ resonator separation.

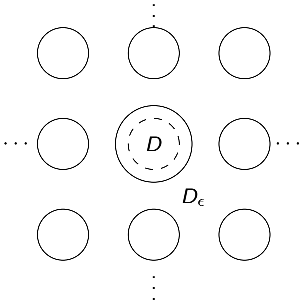

Subwavelength defect modes

- As $\epsilon, \delta \to 0$[11],

$$\omega^{\epsilon} - \omega_* = \exp\left(- \frac{4\pi^2 c_\delta \omega^* R^3}{\delta \epsilon \left(R \|\psi_{\alpha^*}\|^2_{L^2(\partial D)} - 2\mathrm{Cap}_{D,\alpha^*} \right)} + O\left(\frac{1}{\epsilon \ln \delta} + 1 \right) \right);$$

c_δ: positive constant.

- $S(R) = \left(R \|\psi_{\alpha^*}\|^2_{L^2(\partial D)} - 2\mathrm{Cap}_{D,\alpha^*} \right).$

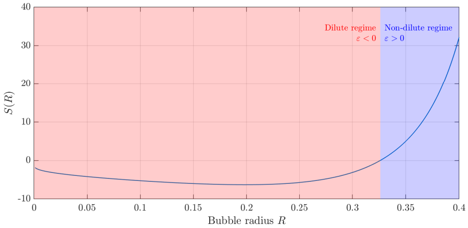

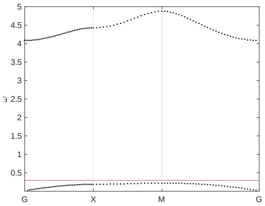

[11] with B. Fitzpatrick, E.O. Hiltunen, S. Yu, SIAM J. Appl. Math., 2018.

Subwavelength defect modes

- Real part of the defect eigenmode:

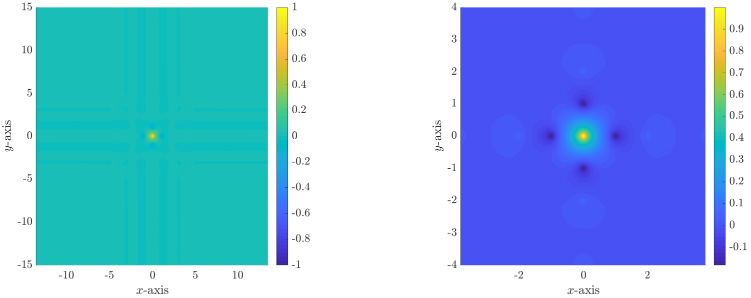

Subwavelength guided modes

- Line defect:[12]

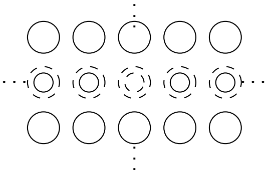

- Defect band within the subwavelength band gap: large perturbation of the radius;
- Defect modes: localized to and guided along the line defect;
- Absence of bound modes.

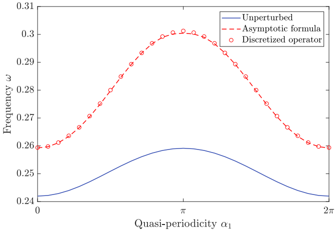

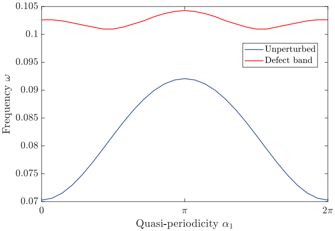

[12] with E.O. Hiltunen, S. Yu, J. Eur. Math. Soc., 2020.

Subwavelength guided modes

- Real part of the defect Bloch eigenfunction for $\alpha_1 = \pi/2$ in the dilute case. Each peak corresponds to one bubble, and the defect line is located at $y = 0$:

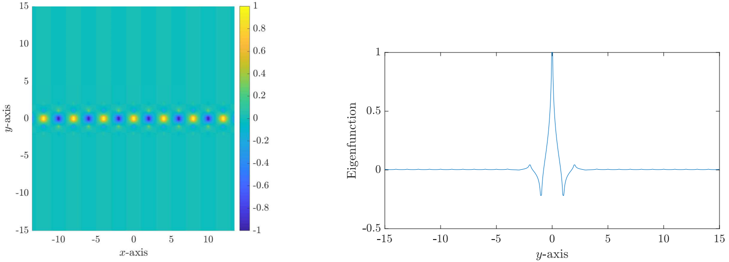

Double-negative metamaterials

- Resonator dimers $\Rightarrow$ double-negative metamaterials[13]:

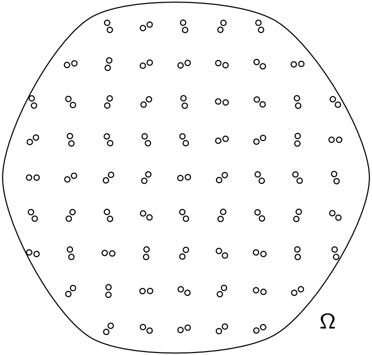

[13] with B. Fitzpatrick, H. Lee, S. Yu, H. Zhang, Quart. Appl. Math., 2019.

Double-negative metamaterials

- Capacitance matrix of $D = D_1 \cup D_2$:

$$C = (C_{ij}), \quad C_{ij} := -\int_{\partial D_j} \psi_i, \quad i,j = 1,2.$$

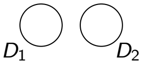

- $\psi_1,\ \psi_2 \in L^2(\partial D)$:

$$\mathcal{S}_D[\psi_1] = \begin{cases} 1 & \text{on } \partial D_1, \\ 0 & \text{on } \partial D_2, \end{cases} \qquad \mathcal{S}_D[\psi_2] = \begin{cases} 0 & \text{on } \partial D_1, \\ 1 & \text{on } \partial D_2. \end{cases}$$

- $\psi_1 \pm \psi_2$: symmetric and anti-symmetric modes.
- Properties of the capacitance matrix:
  - C: positive definite and symmetric.
  - D_1 and D_2 identical balls:
    - $C_{11} = C_{22},\ C_{12} = C_{21},\ C_{11} > 0$, and $C_{12} < 0$.
    - Explicit formulas: bispherical coordinates.

Double-negative metamaterials

- Resonances for a dimer consisting of two identical resonators:
  - Two quasi-static resonances with positive real part for the resonator dimer D.
  - As $\delta \to 0$,

$$\omega_{M,1} = \sqrt{(C_{11} + C_{12})} v_b \sqrt{\delta} - i\tau_1 \delta + O(\delta^{3/2}),$$
$$\omega_{M,2} = \sqrt{(C_{11} - C_{12})} v_b \sqrt{\delta} + \delta^{3/2} \hat{\eta}_1 + i\delta^2 \hat{\eta}_2 + O(\delta^{5/2}).$$

  - $\hat{\eta}_1$ and $\hat{\eta}_2$: real numbers determined by D, v, and v_b;

$$\tau_1 = \frac{v_b^2}{4\pi v}(C_{11} + C_{12})^2.$$

  - Resonances $\omega_{M,1}$ and $\omega_{M,2}$: hybridized resonances of the resonator dimmer D.

Double-negative metamaterials

- Resonator dimer: approximated as a point scatterer with resonant monopole and resonant dipole modes.
- For $\omega = O(\delta^{1/2})$ and $\delta \to 0$, $|x|$: sufficiently large,

$$
\begin{aligned}
u(x) - u^{in}(x) \quad &= \quad \underbrace{g^0(\omega) u^{in}(0) G_k(x,0)}_{monopole} \\
&\quad + \underbrace{\nabla u^{in}(0) \cdot g^1(\omega) \nabla G_k(x,0)}_{dipole} + O(\delta |x|^{-1}).
\end{aligned}
$$

- Scattering coefficients:

$$
g^0(\omega) = \frac{C(1,1)}{1 - \omega_{M,1}^2/\omega^2}(1 + O(\delta^{1/2})), \quad C(1,1) := C_{11} + C_{12} + C_{21} + C_{22};
$$

$$
g^1(\omega) = (g_{ij}^1(\omega));
$$

$$
g_{ij}^1(\omega) = \int_{\partial D} (\mathcal{S}_D^0)^{-1}[x_i](y) y_j - \frac{\delta v_b^2}{\omega^2 |D| (1 - \omega_{M,2}^2/\omega^2)} P^2 \delta_{i,1} \delta_{j,1};
$$

$$
P := \int_{\partial D} y_1 (\psi_1 - \psi_2) d\sigma(y).
$$

Double-negative metamaterials

- Effective medium theory:
  - N: number of resonator dimers; s: characteristic size of a resonator dimer.
  - Assumptions:
    - $sN = \Lambda$ for some positive number $\Lambda > 0$.
    - Volume fraction of the resonator dimers is of the order of $s^3 N$.
    - Resonator dimers: dilute with the average distance between neighboring dimers being of the order of $N^{-1/3}$.

Double-negative metamaterials

- $u^N(x) \to u(x)$ uniformly for $x \in \Omega_N$.
- u: homogenized model

$$\nabla \cdot \underbrace{\left(I - \Lambda \tilde{g}^1 \tilde{B}\right)}_{\text{negative effective } \rho} \nabla u(x) + \underbrace{(k^2 - \Lambda \tilde{g}^0 \tilde{V})}_{\text{negative effective } \kappa} u = 0 \quad \text{in } \Omega.$$

- $\tilde{g}^0$ and $\tilde{g}^1$: Leading-order terms in the monopole and dipole coefficients.
- Resonator dimers distributed s.t. $\tilde{B}$: positive matrix with $\tilde{B}(x) \geq C > 0$ for some constant C for all $x \in \Omega \Rightarrow$ both the matrix $I - \Lambda \tilde{g}^1 \tilde{B}$ and the scalar function $k^2 - \Lambda \tilde{g}^0 \tilde{V}$: negative.
- Effective double-negative medium.

Double-negative metamaterials

- Effective properties:

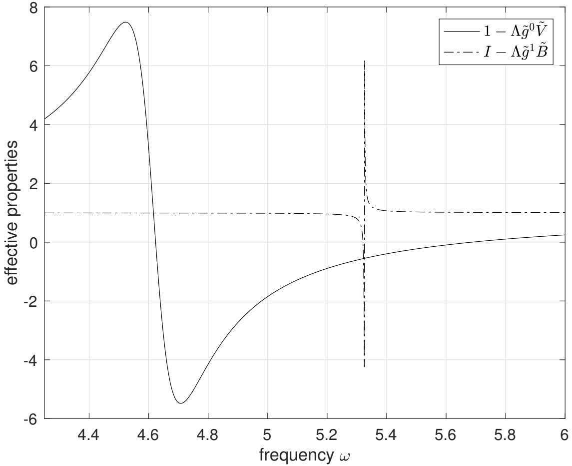

Honeycomb lattice of subwavelength resonators

- Topological properties:

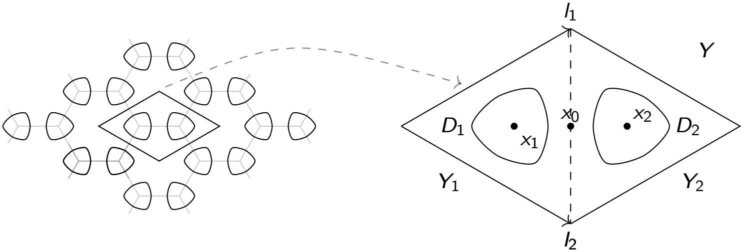

Honeycomb lattice of subwavelength resonators

- Rectangular array of subwavelength dimers:

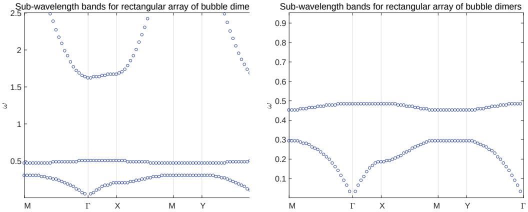

- Honeycomb lattice:

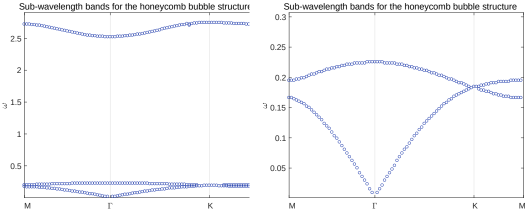

Honeycomb lattice of subwavelength resonators

- At $\alpha = \alpha^*$, the first Bloch eigenfrequency $\omega^* := \omega(\alpha^*)$ of multiplicity 2.
- Conical behavior of subwavelength bands[14]: The first band and the second band form a Dirac cone at α^*, i.e.,

$$\omega_1(\alpha) = \omega(\alpha^*) - \lambda|\alpha - \alpha^*|[1 + O(|\alpha - \alpha^*|)],$$
$$\omega_2(\alpha) = \omega(\alpha^*) + \lambda|\alpha - \alpha^*|[1 + O(|\alpha - \alpha^*|)];$$

  $\lambda = c\sqrt{\delta}\lambda_0 \neq 0$ for sufficiently small δ.

- Dirac point at $\alpha = \alpha^*$.

[14] with B. Fitzpatrick, E.O. Hiltunen, H. Lee, S. Yu, SIAM Math. Anal., 2020.

Honeycomb lattice of subwavelength resonators

- For α close to α^*, Bloch eigenfunctions:

$$\tilde{u}_1(x)S_1(\tfrac{x}{s}) + \tilde{u}_2(x)S_2(\tfrac{x}{s}) + O(\delta + s);$$

- Effective equation: $\tilde{u}_j$ satisfies

$$|c|^2\lambda_0^2\Delta\tilde{u}_j + \underbrace{\frac{(\omega-\omega^*)^2}{\delta}}_{\text{near zero}}\tilde{u}_j = 0.$$

- Single near-zero metamaterial: $1/\kappa$ near zero;
- Transmission without phase change.
- Dirac equation:[15]

$$\lambda_0 \begin{bmatrix} 0 & (-ci)(\partial_1 + i\partial_2) \\ (-\overline{c}i)(\partial_1 - i\partial_2) & 0 \end{bmatrix} \begin{bmatrix} \tilde{u}_1 \\ \tilde{u}_2 \end{bmatrix} = \frac{\omega-\omega^*}{\sqrt{\delta}} \begin{bmatrix} \tilde{u}_1 \\ \tilde{u}_2 \end{bmatrix}.$$

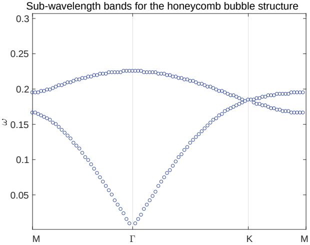

[15] with E.O. Hiltunen, S. Yu, Arch. Ration. Mech. Anal., 2020.

Honeycomb lattice of subwavelength resonators

- One-dimensional plot along the $x-$axis of the real part of the Bloch eigenfunction of the honeycomb lattice shown over many unit cells:

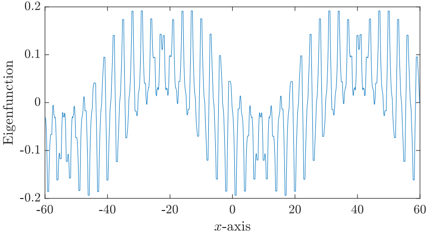

- Square lattice:

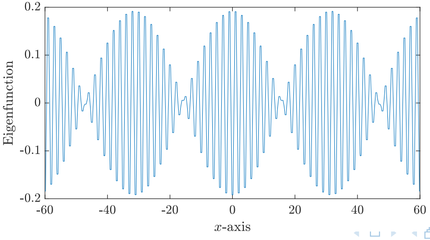

Topological metamaterials

- General principle for trapping and guiding waves at subwavelength scales: introduce a defect to a periodic arrangement of subwavelength resonators.
- Point defect crystal has a localized eigenmode:

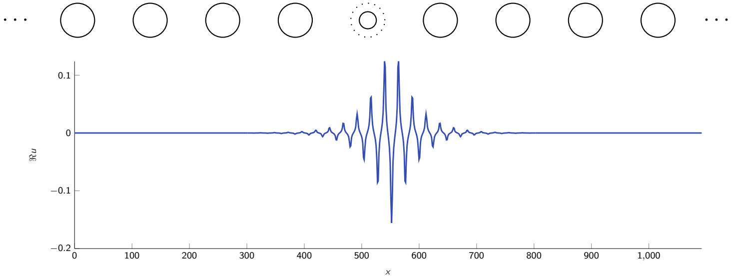

Topological metamaterials

- Sensitivity to imperfections in the crystal's design:

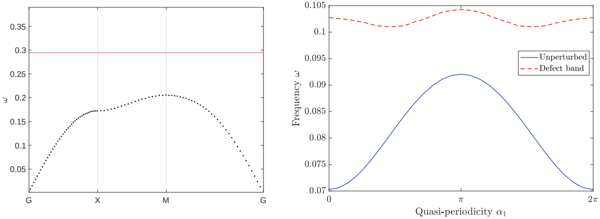

- Goal: design subwavelength wave guides whose properties are robust with respect to imperfections.
- Idea: create a chain of subwavelength resonators that exhibits a robust localized eigenmode.
- Topological invariant which captures the crystal's wave propagation properties.
- Topologically protected edge mode.

Topological metamaterials

- Bulk-boundary correspondence:
  - Take two crystals with topologically different wave propagation properties (different values of the topological invariant);
  - Join half of crystal A to half of crystal B;
  - At the interface, a topologically protected edge mode will exist[16].

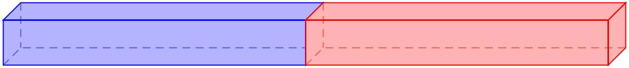

[16] with B. Davies, E.O. Hiltunen, S. Yu, J. Math. Pures Appl., 2020.

Topological metamaterials

- The Zak phase:

$$\varphi_n^z := \int_{Y^*} A_n(\alpha)\, d\alpha; \quad Y^* = \mathbb{R}/2\pi\mathbb{Z} \simeq (-\pi, \pi] \quad \text{(first Brillouin zone)};$$

- Berry-Simon connection:

$$A_n(\alpha) := i \int_D u_n^\alpha \frac{\partial}{\partial \alpha} \overline{u}_n^\alpha \, dx; \quad n = 1, 2.$$

- For any $\alpha_1, \alpha_2 \in Y^*$, parallel transport from α_1 to α_2 gives $u_n^{\alpha_1} \mapsto e^{i\theta} u_n^{\alpha_2}$, where θ is given by

$$\theta = \int_{\alpha_1}^{\alpha_2} A_n d\alpha.$$

- $\Rightarrow$ The Zak phase corresponds to parallel transport around the whole of Y^*.

Topological metamaterials

- An infinite chain of resonator dimers:[17]

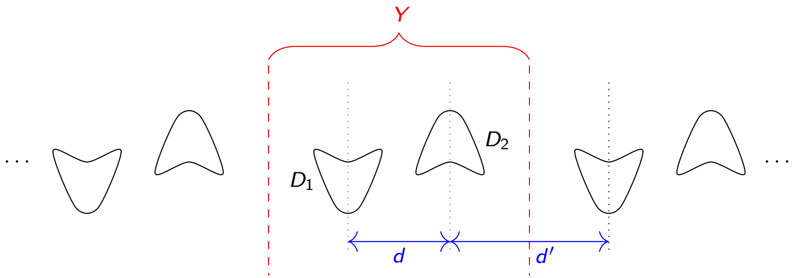

Two assumptions of geometric symmetry:

- dimer is symmetric, in the sense that $D(:= D_1 \cup D_2) = -D$,
- each resonator has reflective symmetry.

[17] Analogue of the Su-Schrieffer-Heeger model in topological insulator theory in quantum mechanics.

Topological metamaterials

- Quasi-periodic capacitance matrix:

$$C_{ij}^{\alpha} := \int_{Y\setminus D} \nabla V_i^{\alpha} \cdot \overline{\nabla V_j^{\alpha}}\, dx, \quad i,j = 1,2;$$

$$\begin{cases} \Delta V_j^{\alpha} = 0 & \text{in} \quad Y\setminus D, \quad D := D_1 \cup D_2; \\ V_j^{\alpha} = \delta_{ij} & \text{on} \quad \partial D_i, \quad \delta_{ij} : \text{the Kronecker delta}; \\ V_j^{\alpha}(x + (mL,0,0)) = e^{i\alpha m} V_j^{\alpha}(x) & \forall m \in \mathbb{Z}, \\ V_j^{\alpha}(x_1,x_2,x_3) = O\left(\frac{1}{\sqrt{x_2^2+x_3^2}}\right) & \text{as } \sqrt{x_2^2+x_3^2} \to \infty, \text{ uniformly in } x_1, \end{cases}$$

- The Zak phase is given by the change in the argument of C_{12}^{α} as α varies over the Brillouin zone:

$$\varphi_n^z = -\frac{1}{2}\left[\arg(C_{12}^{\alpha})\right]_{Y^*}.$$

- Further, it holds that

$$C_{12}^{\alpha}{}' = e^{-i\alpha} C_{12}^{\alpha}, \Rightarrow \text{if } d = d' \text{then } C_{12}^{\pi} = 0,$$

where the prime denotes that d and d' have been swapped.

- Thus,

$$|\varphi_n^{z}{}' - \varphi_n^z| = \pi,$$

i.e. the cases $d > d'$ and $d < d'$ have different Zak phases.

Topological metamaterials

- Dilute computations: Assume that the dimer is a rescaling of fixed domains B_1 and B_2:
$$D_1 = \epsilon B_1 - \left(\frac{d}{2}, 0, 0\right), \quad D_2 = \epsilon B_2 + \left(\frac{d}{2}, 0, 0\right),$$
for $0 < \epsilon$.
- In the dilute regime, as $\epsilon \to 0$:
$$\varphi_n^z = \begin{cases} 0, & \text{if } \ d < d', \\ \pi, & \text{if } \ d > d', \end{cases}$$
- There exists a band gap for all $d \neq d'$,
- The dilute crystal has a degeneracy precisely when $d = d'$.
- The dispersion relation has a Dirac cone at $\alpha = \pi$.
- Band inversion occurs between $d < d'$ and $d > d'$.

Topological metamaterials

- Band inversion:

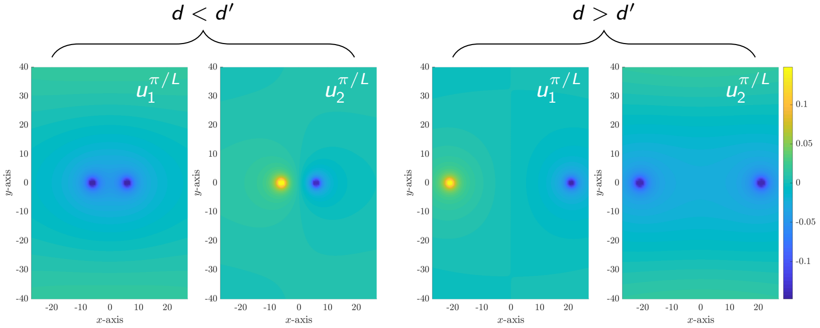

The monopole/dipole natures of the 1st and 2nd eigenmodes have swapped between the $d < d'$ and $d > d'$ regimes.

Topological metamaterials

- A finite chain of resonators

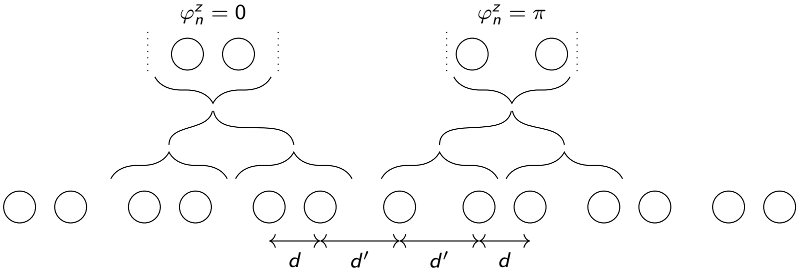

- Capacitance matrix of the finite chain $D = \bigcup_{l=1}^N D_l$:

$$C = (C_{ij}), \quad C_{ij} := -\int_{\partial D_j} (\mathcal{S}_D)^{-1}[\chi_{\partial D_i}], \quad i,j = 1, \ldots, N.$$

- Chiral symmetry: $\Sigma C \Sigma = -C$ $\forall$ Σ s.t. $\Sigma^2 = I$.
- Odd number of resonators $\Rightarrow$ odd number of eigenvalues; middle frequency: midgap frequency $\Rightarrow$ robust to imperfections.

Topological metamaterials

- Finite chain - localisation: There is a localized eigenmode

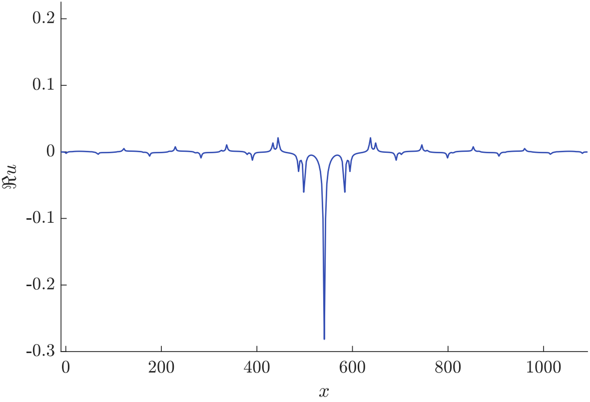

Topological metamaterials

- Finite chain–stability to imperfections: Simulation of band gap frequency (red) and bulk frequencies (black) with Gaussian $\mathcal{N}(0, \sigma^2)$ errors added to the resonator positions. σ: expressed as a percentage of the average resonator separation.
- Even for relatively small errors, the frequency associated with the point defect mode exhibits poor stability and is easily lost amongst the bulk frequencies.
- Due to chiral symmetry, the frequency associated with edge mode occurs in the center of the band gap.

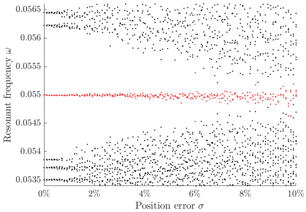

Finite chain with topological interface

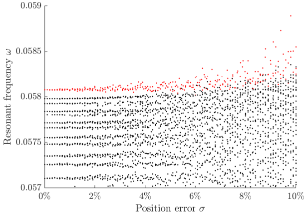

Classical, point defect chain.

Topological metamaterials

- Finite chain - effect of diluteness.
- The variance of each frequency is consistent across both dilute and non-dilute regimes.
- In both the dilute and non-dilute regimes, the structure supports a localized mode whose resonant frequency is in the middle of the band gap.
- In the dilute regime, the nearest-neighborhood approximation, $C_{ij} = 0$ if $|i - j| > 1$ does not give an accurate approximation $\Rightarrow$ significant difference between classical wave propagation problems and topological insulator theory in quantum mechanics.

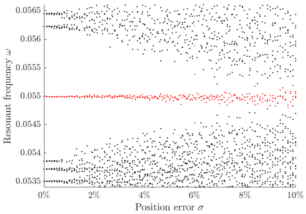

Dilute chain, $d = 12$, $d' = 42$, $R = 1$

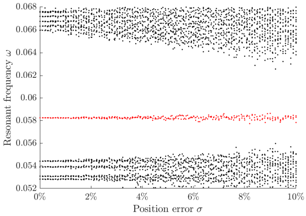

Non-dilute chain, $d = 3$, $d' = 6$, $R = 1$

Topological metamaterials

- Short finite chains: The stable mode exists also in very short chains of subwavelength resonators.
- With only 9 resonators, there is a midgap frequency which is much more stable than the bulk frequencies.

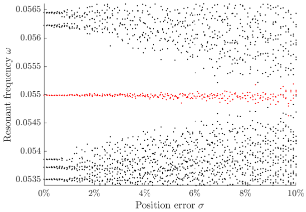

$N = 41$ resonators

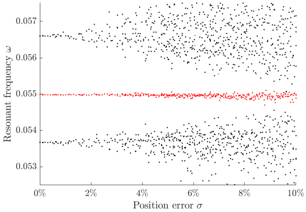

$N = 9$ resonators

Dipolar subwavelength resonances

- u^{in}: incident plane wave; Helmholtz equation:

$$\left\{ \begin{array}{l} \nabla \cdot \Big(\dfrac{1}{\rho} \chi(\mathbb{R}^d \setminus \bar{D}) + \dfrac{1}{\rho_b(\omega)} \chi(\overline{D}) \Big) \nabla u + \omega^2 u = 0, \\ u^s := u - u^{in} \text{ satisfies the outgoing radiation condition.} \end{array} \right.$$

- Uniform small volume expansion[18] with respect to the contrast: $D = z + \delta B$, $\delta \to 0$, $|x - z| \gg 2\pi/k$,

$$u^s = -M(\lambda(\omega), D) \nabla_z G_k(x - z) \cdot \nabla u^{in}(z) + O\Big(\frac{\delta^{d+1}}{\mathrm{dist}(\lambda(\omega), \sigma(\mathcal{K}_D^*))}\Big).$$

- G_k: outgoing fundamental solution to $\Delta + k^2$; $k := \omega\sqrt{\rho}$;
- Polarization tensor:

$$M(\lambda(\omega), D) := \int_{\partial D} x (\lambda(\omega) I - \mathcal{K}_D^*)^{-1}[\nu](x)\, ds(x);$$

  $\lambda(\omega) = (\rho_b(\omega) + \rho)/(2(\rho - \rho_b(\omega)))$.

[18] with P. Millien, M. Ruiz, H. Zhang, Arch. Ration. Mech. Anal., 2017.

Dipolar subwavelength resonances

- Neumann-Poincaré operator $\mathcal{K}_D^*$:

$$\mathcal{K}_D^*[\varphi](x) := \int_{\partial D} \frac{\partial G}{\partial \nu(x)}(x-y)\varphi(y)\, ds(y) \,, \quad x \in \partial D, \nu : \text{normal to } \partial D.$$

- Symmetrization technique for Neumann-Poincaré operator $\mathcal{K}_D^*$:
  - $\mathcal{H}^* = H^{-1/2}(\partial D)$ equipped with the inner product:

$$(u, v)_{\mathcal{H}^*} = -(u, \mathcal{S}_D[v])_{-\frac{1}{2},\frac{1}{2}};$$

  - Calderón's identity: $\mathcal{K}_D \mathcal{S}_D = \mathcal{S}_D \mathcal{K}_D^*$.
- Spectral decomposition formula in $H^{-1/2}(\partial D)$,

$$\mathcal{K}_D^*[\psi] = \sum_{j=0}^{\infty} \lambda_j (\psi, \varphi_j)_{\mathcal{H}^*} \varphi_j.$$

- $\Rightarrow$ Spectral decomposition: (l, m)-entry

$$M_{l,m}(\lambda(\omega), D) = \sum_{j=1}^{\infty} \frac{(\nu_m, \varphi_j)_{\mathcal{H}^*} (\nu_l, \varphi_j)_{\mathcal{H}^*}}{(1/2 - \lambda_j)(\lambda(\omega) - \lambda_j)}.$$

- $(\nu_m, \varphi_0)_{\mathcal{H}^*} = 0$; φ_0: eigenfunction of $\mathcal{K}_D^*$ associated to $1/2$.
- Dipolar subwavelength resonance: $\mathrm{dist}(\lambda(\omega), \sigma(\mathcal{K}_D^*))$ minimal ($\Re e\, \rho_b(\omega) < 0$).

Dipolar subwavelength resonances

- Subwavelength resonances for multiple particles: D_1 and D_2; $\mathrm{dist}(D_1, D_2) > 0$; $\nu^{(1)}$ and $\nu^{(2)}$: outward normal vectors at ∂D_1 and ∂D_2.
- Neumann-Poincaré operator $\mathbb{K}^*_{D_1 \cup D_2}$ associated with $D_1 \cup D_2$:

$$\mathbb{K}^*_{D_1 \cup D_2} := \begin{pmatrix} \mathcal{K}^*_{D_1} & \frac{\partial}{\partial \nu^{(1)}} \mathcal{S}_{D_2} \\ \frac{\partial}{\partial \nu^{(2)}} \mathcal{S}_{D_1} & \mathcal{K}^*_{D_2} \end{pmatrix}.$$

- Symmetrization of $\mathbb{K}^*_{D_1 \cup D_2}$.
- Behavior of the spectrum of $\mathbb{K}^*_{D_1 \cup D_2}$ as $\mathrm{dist}(D_1, D_2) \to 0$:
  - The discrete plasmon spectrum becomes more dense;
  - Convergence to a continuous spectrum at the touching limit;
  - Extreme enhancement and confinement of the field inside the gap between the particles.

Dipolar subwavelength resonances

- Two close-to-touching spheres:
  - Approximate resonance condition:

$$\sum_n (\tau - e^{(2n+1)s})^{-1} = 0.$$

  - $\tau = (\varepsilon_c - 1)/(\varepsilon_c + 1) = 1/(2\lambda)$, $s = \cosh^{-1}(\delta/R)$.
  - Blow-up of ∇u in the gap at the subwavelength resonances[19]:

$$\nabla u = O\Big(\frac{1}{(\delta/R)^{3/2}\ln(R/\delta)} \times \frac{1}{\Im m\lambda(\omega)}\Big).$$

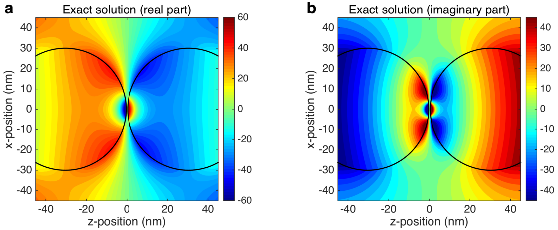

[19] with S. Yu, SIAM Rev., 2018.

Dipolar subwavelength resonances

- Efficient numerical method for a system of close-to-touching plasmonic particles[20].
- Key idea: convert the image charge solution into a Transformation Optics solution.

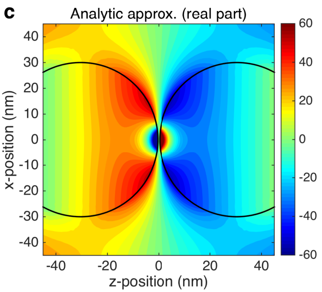

[20]with S. Yu, SIAM Rev., 2018.

Dipolar subwavelength resonances

- Uniform incident field $(0,0,E_0)$ in the direction of the z-axis. In the case of the x or y-axis, a high field concentration in the gap does not happen.
- Method of image charges: infinite series of image charges of strength $\pm u_k$ at $\mathbf{z}_k := (0,0,\pm z_k)$

$$u(\mathbf{r}) = \sum_{k=0}^{\infty} u_k (G(\mathbf{r}-\mathbf{z}_k) - G(\mathbf{r}+\mathbf{z}_k));$$

$\tau = (\varepsilon_c - 1)/(\varepsilon_c + 1) = 1/(2\lambda)$, $s = \cosh^{-1}(\delta/R)$ and $\alpha = R \sinh s$.

$$z_k = \alpha \coth(ks + s + t_0), \quad u_k = \tau^k \frac{\sinh(s+t_0)}{\sinh(ks+s+t_0)}.$$

t_0 s.t. $z_0 = \alpha \coth(s+t_0)$.

- Not valid for spherical resonators due to non-convergence.

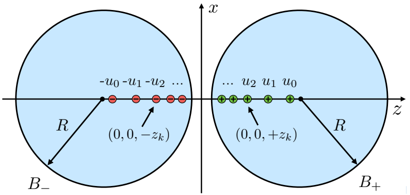

Dipolar subwavelength resonances

- Transformation Optics (TO) basis:

$$\mathcal{M}_{n,\pm}^m(\mathbf{r}) = |\mathbf{r}' - \mathbf{R}_0'|(r')^{\pm(n+\frac{1}{2})-\frac{1}{2}} Y_n^m(\theta', \phi'),$$

  Y_n^m: spherical harmonics.
- TO solution:

$$u(\mathbf{r}) = -E_0 z + \sum_{n=0}^{\infty} A_n \big(\mathcal{M}_{n,+}^0(\mathbf{r}) - \mathcal{M}_{n,-}^0(\mathbf{r})\big).$$

- TO solution: not fully analytic.

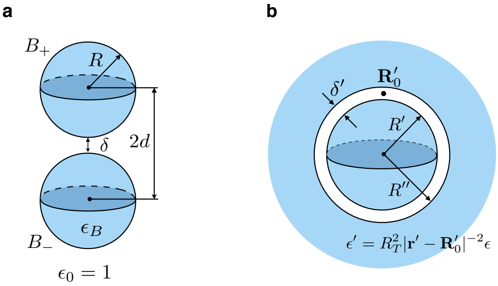

Dipolar subwavelength resonances

- Convert the image charge solution into a Transformation Optics solution: for $\mathbf{r} \in \mathbb{R}^3 \setminus (B_+ \cup B_-)$,

$$u_k G(\mathbf{r} \mp \mathbf{z}_k) = \frac{\sinh(s+t_0)}{4\pi\alpha} \sum_{n=0}^{\infty} \left[\tau e^{-(2n+1)s}\right]^k e^{-(2n+1)(s+t_0)} \mathcal{M}^0_{n,\pm}(\mathbf{r}).$$

- If $|\tau| \approx 1$, the following approximation for the electric potential $V(\mathbf{r})$ holds: for $\mathbf{r} \in \mathbb{R}^3 \setminus (B_+ \cup B_-)$,

$$V(\mathbf{r}) \approx -E_0 z + \sum_{n=0}^{\infty} \widetilde{A}_n \Big(\mathcal{M}^0_{n,+}(\mathbf{r}) - \mathcal{M}^0_{n,-}(\mathbf{r}) \Big); \quad \widetilde{A}_n : \text{explicit}.$$

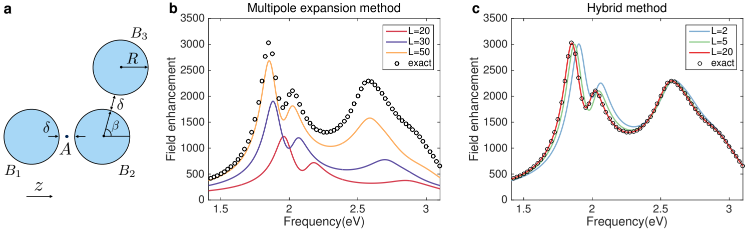

Dipolar subwavelength resonances

- Singular hybridization model for plasmons of strongly interacting many-particle systems[21]:
  - Decomposition of the spectrum into singularly and regularly shifted parts.
  - The singular (resp. regular) part is controlled by local (resp. global) features of the geometry.

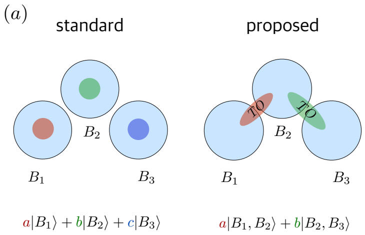

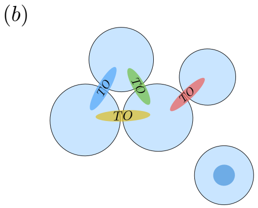

A more general case

[21] with S. Yu, PNAS, 2019.

Dipolar subwavelength resonances

- Coupled mode equations for the hybridization of dimer plasmons:

$$\begin{bmatrix} (\omega_n^{TO})^2 & \Delta_n \\ \Delta_n & (\omega_n^{TO})^2 \end{bmatrix} \begin{bmatrix} a_n \\ b_n \end{bmatrix} = \omega^2 \begin{bmatrix} a_n \\ b_n \end{bmatrix}.$$

- Δ_n: coupling between the two TO modes.
- Spectral theory of the Neumann–Poincaré operator $\Rightarrow$ hybrid modes for the trimer:

$$|\omega_n^{\pm}\rangle \approx \frac{1}{\sqrt{2}}\Big(|\omega_n^{TO}(B_1, B_2)\rangle \mp |\omega_n^{TO}(B_2, B_3)\rangle\Big), \quad n = 1, 2, 3, \cdots,$$

and their resonance frequencies

$$\omega_n^{\pm} \approx \omega_n^{TO} \pm \Delta_n, \quad n = 1, 2, 3, \cdots.$$

- As the bonding angle between the two gap-plasmons decreases, the coupling strength Δ_n increases, which is to be expected since the two gaps get closer.

Dipolar subwavelength resonances

gap distance $\delta = 1.5$ nm

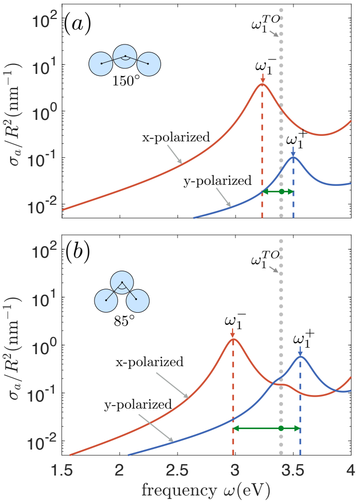

Concluding remarks

- Mathematical and numerical framework for subwavelength wave physics: Focusing, controlling, and guiding waves at subwavelength scales.
- Quantitative explanation of the mechanisms behind the spectacular properties exhibited by subwavelength resonators in recent physical experiments.

Monopolar subwavelength resonances	Dipolar subwavelength resonances
$1/2$: eigenvalue of the Neumann-Poincaré operator	$\lvert\lambda_j\rvert < 1/2$: eigenvalues of the Neumann-Poincaré operator
Eigenspace$(1/2)$: nbr of connected components	$\bigcup_j$ eigenspace(λ_j): orthonormal basis of $\mathcal{H}^*$
Dimer: 2 hybridized resonances Monopole and dipole hybridized modes	Infinite number of hybridized resonances Hybridized modes: multipoles
Double negative metamaterials	Chirality[22]
Gradient blow-up: near the dipole hybridized resonance[23]	near all the hybridized resonances

[22] with W. Wu, S. Yu, Quart. Appl. Math., 2019.
[23] with B. Davies, S. Yu, SIAM MMS, 2020.

Concluding remarks

- Avenue for understanding the topological properties of hermitian and non-hermitian[24,25] systems of subwavelength resonators.

Classical wave problems	Quantum mechanics
PDE model	Hamiltonian
Capacitance matrix: dimer, quasi-periodic, finite chain discrete approximation of the differential problem resonant frequencies & Bloch eigenfunctions	
Dilute regime: approximation of the capacitance matrix	Tight-binding model: Hamiltonian: small correction to sum of Hamiltonians of single isolated atoms
Not accurate: slow decay of the off-diagonal terms of the capacitance matrix	Nearest-neighborhood approximation: Tridiagonal tight-binding matrix

[24]with B. Davies, E.O. Hiltunen, H. Lee, S. Yu, submitted, 2020.
[25]with E.O. Hiltunen, submitted, 2020.

Concluding remarks

- Hair cells: subwavelength resonant elements.
- Fully-coupled subwavelength resonance theory for large, finite systems of size-graded subwavelength resonators and acoustic modelling of passive[26] and active cochlea[27]

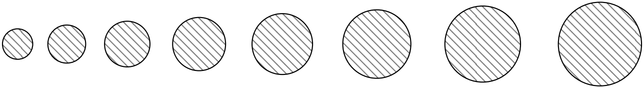

Array of size-graded subwavelength resonators

[26] with B. Davies, Proc. Royal Soc. A, 2019.
[27] with B. Davies, Proc. Royal Soc. A, 2020.

Concluding remarks

- Our model:
  - Predicts the existence of a travelling wave and tonotopic map behaviours in the acoustic pressure distribution in the cochlea fluid, and the behavior of the cochlea amplifier;
  - Unifies the Helmholtz' and Bekesy's models of the cochlea.
  - Can be used as the basis for a machine hearing procedure which mimics neural processing in the auditory system by extracting the global properties of behaviourally significant sounds[28].

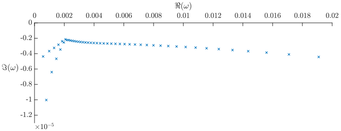

Resonant frequencies

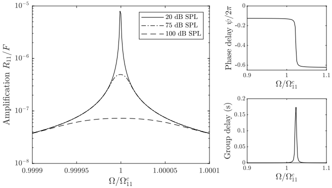

Nonlinear amplification at resonant frequencies

[28] with B. Davies, submitted 2020.